



Enhanced Cu and Cd sorption after soil aging of woodchip-derived biochar: What were the driving factors?



Maria V. Rechberger^{a,b}, Stefanie Kloss^a, Shan-Li Wang^c, Johannes Lehmann^d, Harald Rennhofer^e, Franz Ottner^f, Karin Wriessnig^f, Gabrielle Daudin^g, Helga Lichtenegger^e, Gerhard Soja^{b,h}, Franz Zehetner^{a,*}

^a Institute of Soil Research, University of Natural Resources and Life Sciences, Peter-Jordan-Str. 82, 1190, Vienna, Austria

^b AIT Austrian Institute of Technology GmbH, Energy Department, Environmental Resources & Technologies, Konrad-Lorenz-Str. 24, 3430, Tulln, Austria

^c Department of Agricultural Chemistry, National Taiwan University, Taipei, Taiwan

^d Soil and Crop Sciences, Cornell University, Ithaca, NY 14853, United States

^e Institute of Physics and Material Sciences, University of Natural Resources and Life Sciences, Peter-Jordan-Str. 82, 1190, Vienna, Austria

^f Institute of Applied Geology, University of Natural Resources and Life Sciences, Peter-Jordan-Str. 82, 1190, Vienna, Austria

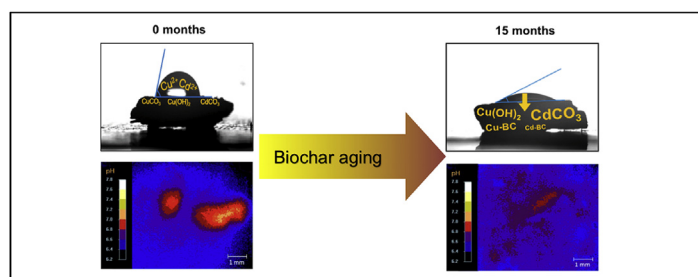
^g Eco&Sols, Univ Montpellier, CIRAD, INRA, IRD, Montpellier SupAgro, Place Viala, 34060, Montpellier, France

^h Institute for Chemical and Energy Engineering, University of Natural Resources and Life Sciences, Muthgasse 107, 1190 Vienna, Austria

HIGHLIGHTS

- Soil aging of biochar increased Cu and Cd sorption capacity.
- Increased access of dissolved metals to biochar pores upon aging.
- Cu was increasingly sorbed to the biochar organic phase upon aging.
- Cd was predominantly bound as CdCO₃ on the biochars even after aging.

GRAPHICAL ABSTRACT



ARTICLE INFO

Article history:

Received 6 June 2018

Received in revised form

12 October 2018

Accepted 15 October 2018

Available online 24 October 2018

Handling Editor: Patryk Oleszczuk

Keywords:

Biochar aging

ABSTRACT

Biochar (BC) is increasingly tested as a soil amendment for immobilization of heavy metals (HMs) and other pollutants. In our study, an acidic soil amended with wood chip-derived BC showed strongly enhanced Cu and Cd sorption after 15 months of aging under greenhouse conditions. X-ray absorption near edge structure suggested formation of Cu(OH)₂ and CuCO₃ and upon aging increasingly Cu sorption to the BC organic phase (from 9.2% to 40.7%) as main binding mechanisms of Cu on the BCs. In contrast, Cd was predominantly bound as CdCO₃ on the BCs even after 15 months (82.7%). We found indications by mid-infrared spectroscopy that the formation of organic functional groups plays a role for increased HM sorption on aged BCs. Yet, our data suggest that the accessibility of BC's pore network and reactive surfaces is likely to be the overriding factor responsible for aging-related changes in HM sorption capacity, rather than direct interactions of HMs with oxidized functional groups. We observed highly

Abbreviations: BC, Biochar; BET, Brunauer-Emmett-Teller; CEC, Cation exchange capacity; EC, Electrical conductivity; EP, Error parameters; HM, Heavy metal; LCF, Linear combination fitting; MIR, Mid-infrared; SA, Surface area; SSA, Specific surface area; SAXS, Small angle X-ray scattering; SEM, Scanning electron microscopy; TG-DSC, ThermoGravimetry - Differential scanning calorimetry; XANES, X-ray absorption near edge structure; XAS, X-ray absorption spectroscopy.

* Corresponding author.

E-mail address: franz.zehetner@boku.ac.at (F. Zehetner).

Heavy metal
Copper
Cadmium
Contact angle
XANES

weathered BC surface structures with scanning electron microscopy along with strongly increased wettability of the BCs after 15 months of soil aging as indicated by a decrease of water contact angles (from 62.4° to 4.2°).

© 2018 Elsevier Ltd. All rights reserved.

1. Introduction

Heavy metal (HM) contaminated soils can occur naturally but are increasingly caused by human activity such as mining, smelting, transportation, waste disposal, combustion of waste and fossil fuels as well as application of fertilizers (Ali et al., 2013; Álvarez et al., 2018; Jarup, 2003). Cu is widely used for pest control in viticulture as well as in the production of fruits and potatoes and may accumulate in soils (Lamichhane et al., 2018). Cu is a micronutrient and therefore beneficial at lower concentrations; however, soil microbial communities and earthworms are especially sensitive to higher Cu concentrations (Komárek et al., 2010). Cu strongly interacts with organic substances in the soil. It is less mobile than Cd; however, it may still be mobilized by forming soluble organic complexes and be taken up by plants and animals (Brun et al., 2001). At lower pH, Cu is predominantly bound to organic functional groups while at high pH, mineral precipitation is predominant (Komárek et al., 2010). Cd accumulation is of major concern in agricultural soils due to its steady input through application of phosphate fertilizers containing Cd impurities, sludges and composts (Cheraghi et al., 2012). Cd is highly toxic to humans and shows high mobility and plant uptake.

Due to the high mobility of Cd and the high input of Cu in the environment, remediation methods for Cd and Cu contaminations are needed. Especially in acidic soils, Cd and Cu toxicity and contamination of the groundwater is of major concern due to elevated HM mobility. HM extraction e.g. through phytoremediation is not always feasible, and the application of biochar (BC) may be an alternative for in-situ soil remediation by HM immobilization. Based on the typical features of BC to increase CEC and pH in the soil, BC is currently investigated for remediation purposes of contaminated soils and water (Blackwell et al., 2009; Uchimiya et al., 2010). Under acidic conditions, crop straw-derived BC was found to be more effective in removing Cu²⁺ from an aqueous solution than activated carbon (Tong et al., 2011). Water-soluble Cd²⁺ could be reduced 10-fold (Beesley et al., 2010) and 300-fold (Beesley and Marmiroli, 2011) after wood-derived BC application to a contaminated soil, and sorption was identified as an effective mechanism for this. The extent of HM sorption to BC-treated soils is dependent on BC properties such as the O/C ratio and the persistence of BCs as well as on BC effects in the soil including changes in pH and dissolved organic matter content (Sauvé et al., 2000; Uchimiya et al., 2012). Increased dissolved organic carbon content has been found to enhance Cu mobilization after BC amendment (Beesley et al., 2010).

In addition, BC aging in the soil leads to BC surface oxidation and the formation of oxygen-containing functional groups (Cheng et al., 2008, 2006), which may influence metal sorption behavior (Toles et al., 1999; Uchimiya et al., 2012). However, Li et al. (2016) observed reduced Cu and Cd sorption abilities of hardwood-derived BCs within 3 years after addition to a paddy soil. In another experiment, adsorption isotherms showed elevated Cd sorption in an Oxisol and an Inceptisol after amendment with aged wood BCs (12 months aging in the respective soils at 40 °C) in comparison to the fresh BCs (Nagodavithane et al., 2014). The authors could not specify the mechanisms behind the increased HM

sorption of the aged BC, but excluded changes in pH and CEC as possible driving factors as both did not change significantly.

The aim of our study was, therefore, to identify the mechanisms responsible for changes in Cu and Cd sorption upon aging of biochar. We hypothesized that (1) BC aging leads to increased accessibility of the BC pores for soil solution allowing increased HM sorption and that (2) the sorption of Cu and Cd on BC surfaces increasingly involves bonding to organic sites as functionality increases with oxidation of BC surfaces upon aging.

2. Materials and methods

2.1. Soil and biochar

The materials were obtained from a pot experiment described in detail in Kloss et al. (2015). Briefly, mixed wood chips (wood from ash tree [*Fraxinus excelsior*] and poplar [*Populus x canadensis*], wood and needles from spruce [*Picea abies*]) were pyrolyzed under Ar atmosphere in a rotary furnace at a highest treatment temperature of 525 °C (residence time 60 min). The BC was aged for 15 months in an acidic sandy loam Planosol in a pot experiment under greenhouse conditions. BC and soil characteristics are summarized in Table 1. The experiment was comprised of pots containing soil mixed with BC (particle size <5 mm) at 3 w.-% application rate and controls containing soil only. This application rate corresponds to a BC application of 90 t ha⁻¹ at a plowing depth of 20 cm and lies in the upper range of field experiments (Watzinger et al., 2014; Woolf et al., 2010). Mustard (*Sinapsis alba* L.), barley (*Hordeum vulgare* L.) and red clover (*Trifolium pratense* L.) were grown consecutively in the pots. The experiment was run under semi-controlled temperature conditions simulating a day–night temperature profile with temperatures ranging from 14 °C to 25 °C (Kloss et al., 2015).

After 15 months, the soils were air-dried, and from an aliquot, BC pieces were manually isolated. To remove clay particles from the BC surface, the BCs were treated with ultrasonication, washed and sieved at 200 µm, dried for 24 h at 60 °C and stored under ambient air. The same pre-treatment was performed for fresh BC.

Table 1

Characterization of the wood chip biochar and the soil (Planosol) used in the pot experiment. Values are reported as means ± standard deviation (n = 3). Modified from Kloss et al. (2015).

	Biochar	Planosol
Pyrolysis temperature	525 °C	
Ash content [w.-%]	15.2	
BET-N ₂ SA [m ² g ⁻¹]	26.4 ± 1.0	
pH (CaCl ₂)	8.9 ± 0.1	5.4 ± 0.0
EC [mS cm ⁻¹]	1.58 ± 0.2	0.04 ± 0.01
CEC [mmol _c kg ⁻¹]	93.0 ± 1.9	75.1 ± 0.0
Carbonate [%]	1.85 ^a	0.0 ± 0.0
OC [%]	67.1 ± 1.3	1.64 ± 0.04
Clay [%]		10.7
Sand [%]		69.8

^a Obtained by thermogravimetry; EC = electrical conductivity, liquid; solid = 10:1; CEC = cation exchange capacity; BET-N₂ SA = Brunauer-Emmett-Teller - N₂ surface area; OC = organic carbon content.

2.2. Cu and Cd sorption experiments on fresh and aged soil-biochar mixtures

Cu and Cd sorption experiments were carried out with fresh and aged soil-BC mixtures using the same methods as already described in Kloss et al. (2015). Briefly, 4 g of soil-BC mixture (or control without BC) ($n = 3$) was treated for 24 h with 40 mL of HM solution containing eight different concentrations of Cu (0–400 mg L⁻¹) or Cd (0–200 mg L⁻¹), respectively, with 0.01 M CaCl₂ as background electrolyte. The filtrate was stabilized with 65% HNO₃, and the remaining Cu and Cd concentrations were measured by atomic absorption spectroscopy (Buck Scientific® Atomic Absorption Spectrometer Model 210 VGP). Sorption isotherms were obtained by plotting the concentration of sorbed HM against the equilibrium concentration in solution.

2.3. Cu and Cd spiking of fresh and aged biochar particles

In order to further investigate Cu and Cd sorption mechanisms on BC, fresh and aged BC pieces were treated with Cu (5 and 100 mg L⁻¹) and Cd (15 and 300 mg L⁻¹) solutions with 0.01 M CaCl₂ as background electrolyte. To this end, 0.05 g of BC was weighed into 20 mL polypropylene flasks and treated with 10 mL solution. The pH was adjusted to 4 and 6.3, respectively, using dilute HCl and NaOH in order to cover the pH range of the soil sorption isotherm experiments. Before shaking, the samples were evacuated for 15 min to facilitate contact of the BC pores with the solution. Adjustment of pH was carried out several times between shaking; altogether, the samples were shaken for 24 h, pH adjusted once again and then filtered with membrane filters (0.1 μm). The BCs on the filter membrane were washed several times with distilled water using a syringe. The highest loading concentration of Cd exceeds the usual concentrations of experiments (Rizwan et al., 2018); however, this was necessary for X-ray absorption spectroscopy (XAS).

2.4. Analyses performed on fresh and aged biochar particles without metal spiking

Contact angle was measured to assess the hydrophobicity/wettability of the BC surfaces. To this end, a droplet of double distilled water was applied with a manual dosage system on BC pieces ($n = 7$) with an even surface of at least 2–3 mm length and width. Contact angle measurements were carried out 10 s after the application of the droplet. If the droplet was absorbed within 10 s, the contact angle was counted as 0° (Rechberger et al., 2017). To evaluate the droplet images, sessile drop shape analysis was performed using the software DSA1 (Krüss® GmbH).

Specific surface area (SSA) was estimated by measuring the monolayer water adsorption at a defined relative humidity ($p/p_0 = 0.19$), a method established by Quirk (1955) and successfully tested for biochars (Fang et al., 2010). Briefly, 0.25 g of dried BC (60 °C, $n = 3$) was placed in a desiccator over a saturated CaBr₂ solution at 20 ± 0.1 °C until constant weight was reached. The SSA was calculated from the amount of adsorbed water assuming that the space occupied by a molecule in the H₂O monolayer is 0.108 nm² [22].

In situ pH measurements were conducted using fluorescent pH sensor foils (product code SF-HP51R), a fluorescence microscope device (VisiSens A2) and VisiSens AnalytiCal 2 software (all from PreSens® GmbH, Regensburg, Germany). 10 point-calibration was carried out with phosphate-buffered saline containing disodium phosphate, monosodium phosphate and NaCl in the pH range of 4.5–9. Ionic strength for calibration was adjusted to 75 mM based on the EC of the soil and using the calculation of Alva et al. (1991).

To obtain EC, the soil was diluted with double distilled water until a saturation paste was obtained little above water holding capacity (WHC) (Hoefer et al., 2017). After horizontal shaking for 2 h (Edmund Bühler® SM-30; 75 rpm), the soil paste was left over night and then centrifuged for 10 min (Sorvall® RC 5C Plus Centrifuge; SS 34 rotor; RCF = 17 211 g). In the supernatant, EC was measured with a WTW inoLab conductivity meter. For equilibration, the optodes were soaked for 180 min in 150 mM phosphate-buffered saline and rinsed prior to the measurements. 34 g of soil was filled in a polystyrene petri dish to occupy a volume of 21.6 cm³ and moistened to 60% WHC to ensure similar bulk densities among samples. BC pieces were placed onto the soil, moistened and measured with the pH optodes after 2 h.

Scanning electron microscopy (SEM) of fresh and aged BC particles was performed using a Quanta 250 FEG (FEI Company®) with an Everhart Thornley detector. Measurements were carried out at 10 kV in high-vacuum mode.

Small angle X-ray scattering (SAXS) was performed to gain information on the nanostructure of the fresh and aged BC samples. Measurements were carried out with a 3-pinhole SMAX-3000 SAXS camera (RIGAKU®) equipped with a MM002+ X-ray source (with copper target wavelength of $\lambda = 0.1541$ nm). Two-dimensional scattering images were recorded with a TRITON® 200 multi-wire X-ray detector (200 mm diameter mapped on 1024 × 1024 pixels). For the measurement, ground BC was placed between two layers of adhesive tape. The scattering pattern was integrated, background subtracted and the resulting curve was interpreted according to Pfeifer et al. (2002) and Wachha et al. (2011). Specifically, the radius of Gyration related to the size of pores in the nanometer regime and the power law exponent attributed to the surface roughness of the nanostructures were calculated according to methods described in detail in Rechberger et al. (2017).

X-ray diffraction was performed on ground BC samples using a Panalytical XPertPro MPD (Panalytical®, Almelo, Netherlands) diffractometer with automatic divergent slit, copper anode, long fine focus tube (45 kV, 40 mA), and an X'Celerator detector. The measuring time was 25 s, with a step size of 0.017°2θ. The results were qualitatively evaluated using the software PANalytical X'Pert HighScore Plus Version 3.0.

Thermogravimetry - differential scanning calorimetry (TG-DSC) was carried out using a STA 409 PG Luxx (Netzsch®, Germany) instrument under air atmosphere (100 mL min⁻¹) with 20 mL min⁻¹ N₂ as protective gas. Approx. 5 mg of ground BC sample was used for the measurement. Heating rate was 5 °C min⁻¹ and measurement was carried out in the temperature range from 22 °C to 1000 °C.

Mid-infrared (MIR) spectroscopy was conducted on ground BC samples. 200 mg KBr pellets were made with 0.5% (= 1 mg) BC. MIR spectroscopy was carried out with a 4 cm⁻¹ resolution measuring the absorbance from 4000 to 400 cm⁻¹ (32 scans per sample; Tensor 27 SN 1683; Bruker®). For each sample, 3 KBr pellets were made; the obtained spectra were vector normalized and then averaged using OPUS (version 6.5) software.

2.5. Analyses performed on fresh and aged biochar particles after Cu and Cd sorption

MIR spectroscopy was also conducted on BC samples that had been equilibrated with Cu and Cd solutions, respectively, at pH 4 and 6.3 (s. above). Samples treated at pH 4 were additionally analyzed by X-ray absorption spectroscopy (XAS) at the National Synchrotron Radiation Research Center in Hsinchu, Taiwan. Cd and Cu K-edge XAS analyses were conducted at beamlines 01C and 17C, respectively. The spectra were collected in fluorescence mode using a Lytle detector with a set of Soller slits and a 6-μm Ag or Ni filter for

Cd or Cu, respectively. At least three scans were collected and averaged for each sample and the spectrum of a metallic Cd or Cu film was simultaneously collected in each scan for energy calibration (Cu: 8979 eV; Cd: 26711 eV). After baseline correction and normalization, X-ray absorption near edge structure (XANES) of each spectrum was extracted for linear combination fitting (LCF) using the Athena software (Ravel and Newville, 2005) and a set of reference spectra. The reference compounds included $\text{Cu}(\text{OH})_2$, CuCO_3 and $\text{Cu}(\text{II})$ adsorbed on a BC reference (see supporting information) for the LCF of Cu-containing samples and $\text{Cd}(\text{OH})_2$, CdCO_3 and $\text{Cd}(\text{II})$ adsorbed on a BC reference (see supporting information) for the LCF of Cd-containing samples. To avoid overfitting with a large number of reference compounds, the LCF procedure was first performed for each XANES spectrum using the sets of any three reference compounds and no energy shifts in the reference spectra were permitted in the LCF algorithm. The goodness of a fit was evaluated using the error parameters (EPs) of different fits, defined as $\Sigma(\text{data-fit})^2/(\text{data})^2$ (see Athena Users' Manual for details), where data points are summed over the data points in the fitting region.

Statistical analyses were performed in R, version 3.0.2. If not stated otherwise, values are given as means \pm standard errors.

3. Results and discussion

3.1. Cu and Cd sorption to biochar-amended soils

Metal sorption isotherms (Fig. 1) showed that Cd sorption strongly increased 15 months after BC application whereas sorption on the initial soil-BC mixture was only slightly higher than in the control. Cu sorption showed similar patterns, but with a less pronounced aging effect. While the observed increase in Cu sorption upon aging of the soil-BC mixtures might be explained by a slight pH increase (Fig. 1), significantly higher Cd sorption after 15 months aging was observed at lower pH (5.9) in comparison to fresh soil-BC mixtures (6.3). Therefore, BC aging is likely to have altered the Cd sorption behavior by other mechanisms not reflected in bulk suspension pH, which are discussed in the following sections.

3.2. Aging effects on biochar properties

Aging-induced changes in basic properties (e.g. pH, EC, CEC) of the studied soil-BC mixtures have been discussed in prior studies (Kloss et al., 2014). In this study, planar pH optode measurements displayed the spatial distribution of pH around fresh and aged BC pieces in the studied Planosol (Fig. 2, showing two representative examples). Fresh BCs increased the pH from <6.4 in the surrounding soil to pH 7 on and near BC particles. As the measurement range of the sensor foils started only around 6.2, the surrounding soil is expected to be more acidic than shown by the optodes (pH in CaCl_2 was 5.4). Interestingly, the aged BC still showed a pH increase on and near the BC particles to around pH 6.8. Fig. 2 demonstrates the spatial pH gradients around BC particles, which had been sustained for many months after BC application in our study and indicate a completely different chemical environment for HM sorption in proximity to BC particles compared to the bulk soil. Indeed, metal hydroxide (surface) precipitation seems possible on/near the BCs even though the bulk pH would not indicate this to be likely.

SEM of isolated BC pieces showed signs of weathering and disruption of the BC surfaces after aging in soil. Fig. 3 depicts two exemplary micrographs of the 18 analyzed samples. The surface alterations seen in Fig. 3 may be the visible expression of underlying changes in physico-chemical surface properties upon aging in the soil.

Indeed, we found that water contact angle on BC surfaces decreased from $62.4 \pm 4.8^\circ$ to $4.2 \pm 1.5^\circ$ after 15 months of soil aging indicating rapid development of highly hydrophilic properties on the BC surfaces (Table 2). In a similar study, decreasing water contact angles on BCs derived from willow wood were correlated with the formation of carboxylic and other acidic functional groups after lab incubation in an acidic soil for 2 years (Rechberger et al., 2017). Additionally, leaching and microbial degradation of hydrophobic tars (Das and Sarmah, 2015) as well as interaction with soil organic matter may (Hagemann et al., 2017) have increased wettability.

The SSA calculated from water adsorption (Table 2) was higher than the BET N_2 -SA ($26.4 \pm 1.0 \text{ m}^2 \text{ g}^{-1}$; Table 1), which is in agreement with other studies (Fang et al., 2010; Quirk and Murray, 1999); the N_2 molecule is known not to penetrate smaller pores. The BC's water-SSA increased from 88.6 ± 2.5 to $108.1 \pm 2.9 \text{ m}^2 \text{ g}^{-1}$ upon aging, which indicates that the surface area accessible for aqueous solutions and available for the sorption of dissolved substances has increased.

The radius of Gyration related to the size of pores in the nanometer regime and the power law exponent n attributed to the surface roughness of the nanostructures were evaluated using SAXS (Table 2). The scattering curves (not shown) were similar in shape for fresh and aged BCs, featuring the same surface roughness, while the structure feature was shifted for aged BCs. During BC aging, the dominant pore radius in the nanometer regime grew from 2.4 nm to 3.1 nm. Growing pores may have further contributed to the accessibility of the BC pore network for soil solution due to removal and reorganization of (hydrophobic) tars (Das and Sarmah, 2015; Sahouli et al., 1996; Yi et al., 2015), removal of pore clogging mineral phases (Conte and Nestle, 2015) as well as collapsing of BC structures (Gibaud et al., 1996).

In our study, the hydrophobic nature of the fresh BCs likely excluded large portions of their pore network and reactive surfaces from interaction with the soil solution. In line with our hypothesis 1, we propose that as their pores and reactive surfaces become increasingly accessible for soil solution with aging, the BCs become more important for HM sorption, especially in light of their still elevated pH regime (cf. Fig. 2).

The MIR spectra (Fig. 4) revealed the BCs' high aromaticity with pronounced bands at 875, 817 and 753 cm^{-1} assigned to out-of-plane deformation of aromatic C–H, a band at 3030 cm^{-1} assigned to C–H stretching and a peak around 1430 cm^{-1} assigned to aromatic C=C stretching (Guo and Bustin, 1998; Keiluweit et al., 2010; Tatzber et al., 2007). Advanced aromaticity due to the relatively high charring temperature is also reflected by only faint expression of the two bands between 2980 and 2820 cm^{-1} characteristic for aliphatic C–H stretching (Guo and Bustin, 1998; Stevenson, 1994). The presence of carbonates is indicated by a sharp peak at 875 cm^{-1} (assigned to C–O out-of-plane bending) and a band at 1430 cm^{-1} , which is assigned to C–O stretching (Kloss et al., 2012; Socrates, 2001). This observation was confirmed by XRD showing distinct calcite peaks (data not shown). Various bands overlapping in the fingerprint region from 1300 to 1000 cm^{-1} assigned to C–O bonds (Guo and Bustin, 1998; Rumpel et al., 2001; Smith, 1980) and phenolic O–H (Guo and Bustin, 1998) reflect the BCs' diversity of organic compounds and group functionality. A distinctive peak at 1693 cm^{-1} has previously been assigned to carbonyl C=O stretching present in carboxylic functional groups as well as ester, ketones and aldehyde groups (Haberhauer and Gerzabek, 1999; Kaal et al., 2012; Stevenson, 1994). The band at 1575 cm^{-1} may be assigned to aromatic C=C (Chia et al., 2012; Guo and Bustin, 1998; Koch, 1998) and C=O stretching conjugated ketones and quinones (Keiluweit et al., 2010).

After 15 months of BC aging, bands between 1300 and

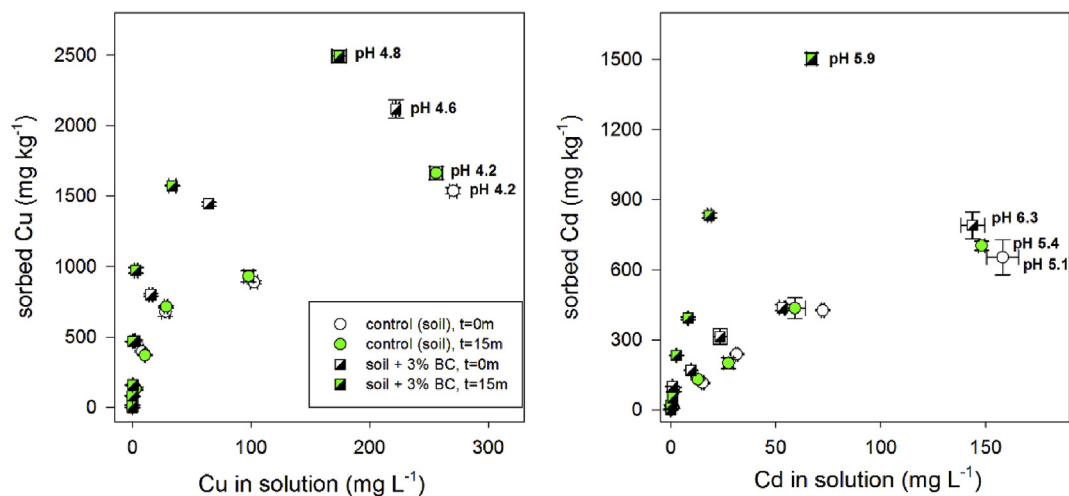


Fig. 1. Copper (left) and cadmium (right) sorption isotherms of wood chip biochar (BC) amended soils ($n=3$; application rate 3 w.-%) 0 and 15 months (m) after application and respective controls (soil only) with pH values of the filtrate at highest concentration. Error bars indicate the standard errors.

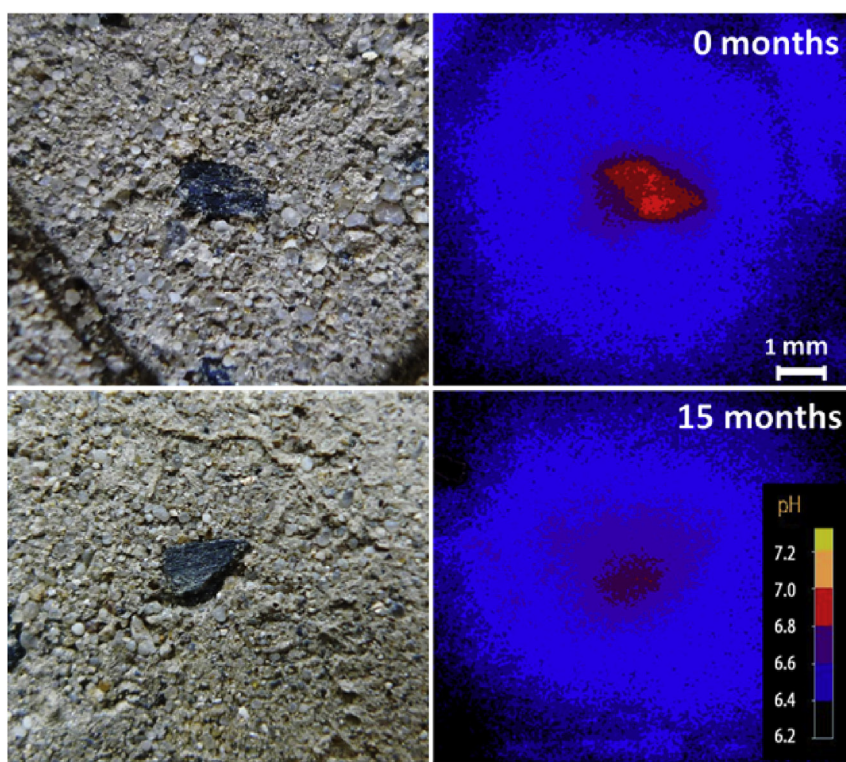


Fig. 2. Planar pH optode measurements of biochar pieces before (0 months) and after aging (15 months) in soil with respective photographs on the left side.

1000 cm^{-1} , at 1575 cm^{-1} and at 1693 cm^{-1} became more pronounced, which suggests oxidation processes creating increased functionality by formation of carboxylic and phenolic groups among others. While the creation of hydrophilic functional groups upon aging was correlated with increased wettability (Rechberger et al., 2017), a recent study suggested that highly hydrophilic surface properties could slow down water flow in micropores ($<0.5\text{ }\mu\text{m}$) retarding sorption processes (Conte and Schmidt, 2017). Along these lines, sorption of perchlorate was positively correlated with the biochar's hydrophobicity and aromatic properties (Fang et al., 2014). The spectrum of the aged BC showed decreased peak heights at 875 cm^{-1} and 1430 cm^{-1} indicating loss of CaCO_3 . From

the TG curves, we estimated a carbonate loss of approx. 60% during the 15 months of BC aging as indicated by the mass loss associated with an endothermic reaction in the DSC curves in the range of $600\text{--}750\text{ }^\circ\text{C}$ (Fig. 5).

Both DSC curves showed a broad exothermic peak around $500\text{ }^\circ\text{C}$ indicative of organic matter combustion; the peak of the aged BC was at higher temperature ($505\text{ }^\circ\text{C}$) than the one of fresh BC ($479\text{ }^\circ\text{C}$), indicating higher aromaticity of the aged BC (Barros et al., 2007). Mass loss in the range of $22\text{--}225\text{ }^\circ\text{C}$ was approx. 35% higher for aged BC than for fresh BC. This may be attributed to stronger hydrophilicity and hence higher uptake of air moisture in the aged BC.

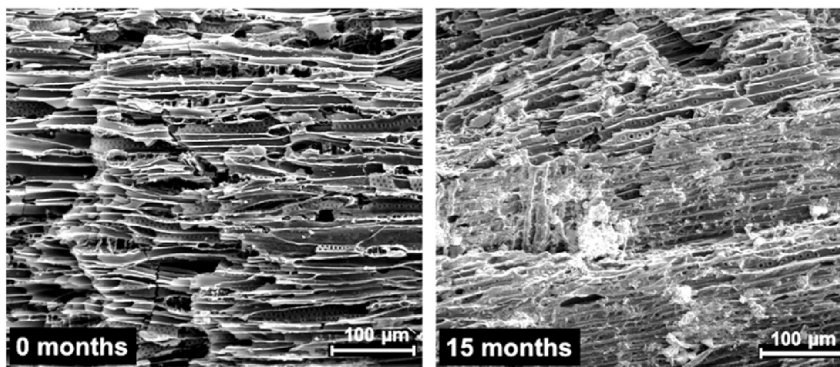


Fig. 3. SEM micrographs of wood chip biochars before (0 months) and after aging (15 months) in soil.

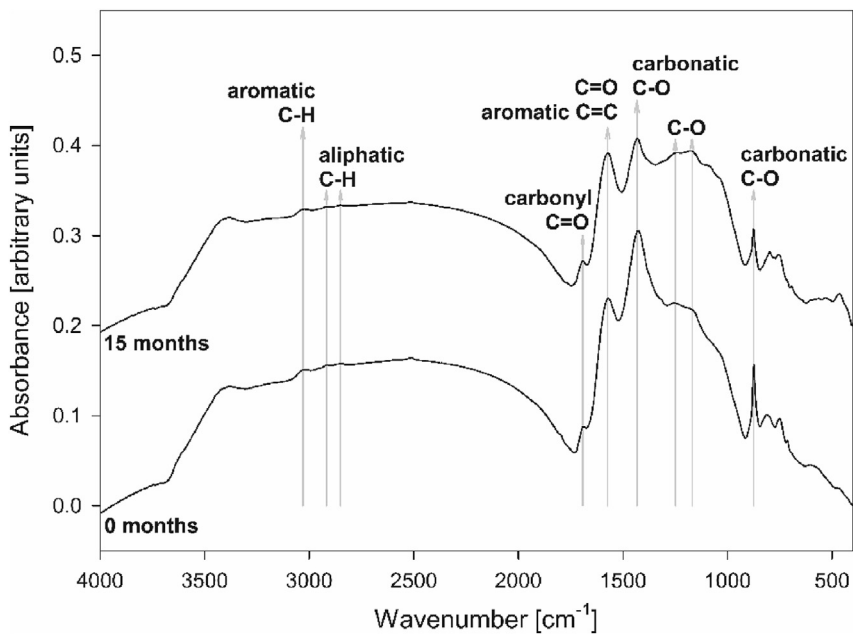


Fig. 4. MIR spectra of wood chip biochar before (0 months) and after aging (15 months) in soil.

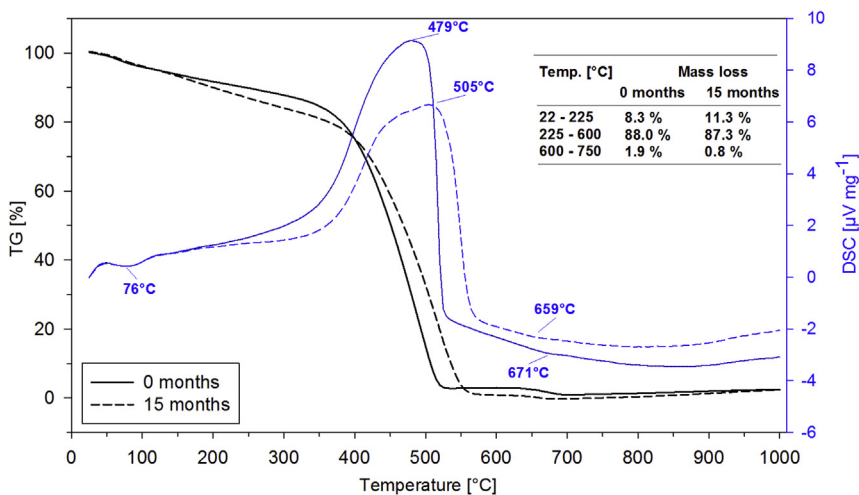


Fig. 5. Thermogravimetric (TG, black) and differential scanning calorimetric (DSC, blue) curves of wood chip biochar before (0 months) and after aging (15 months) in soil. (For interpretation of the references to colour in this figure legend, the reader is referred to the Web version of this article.)

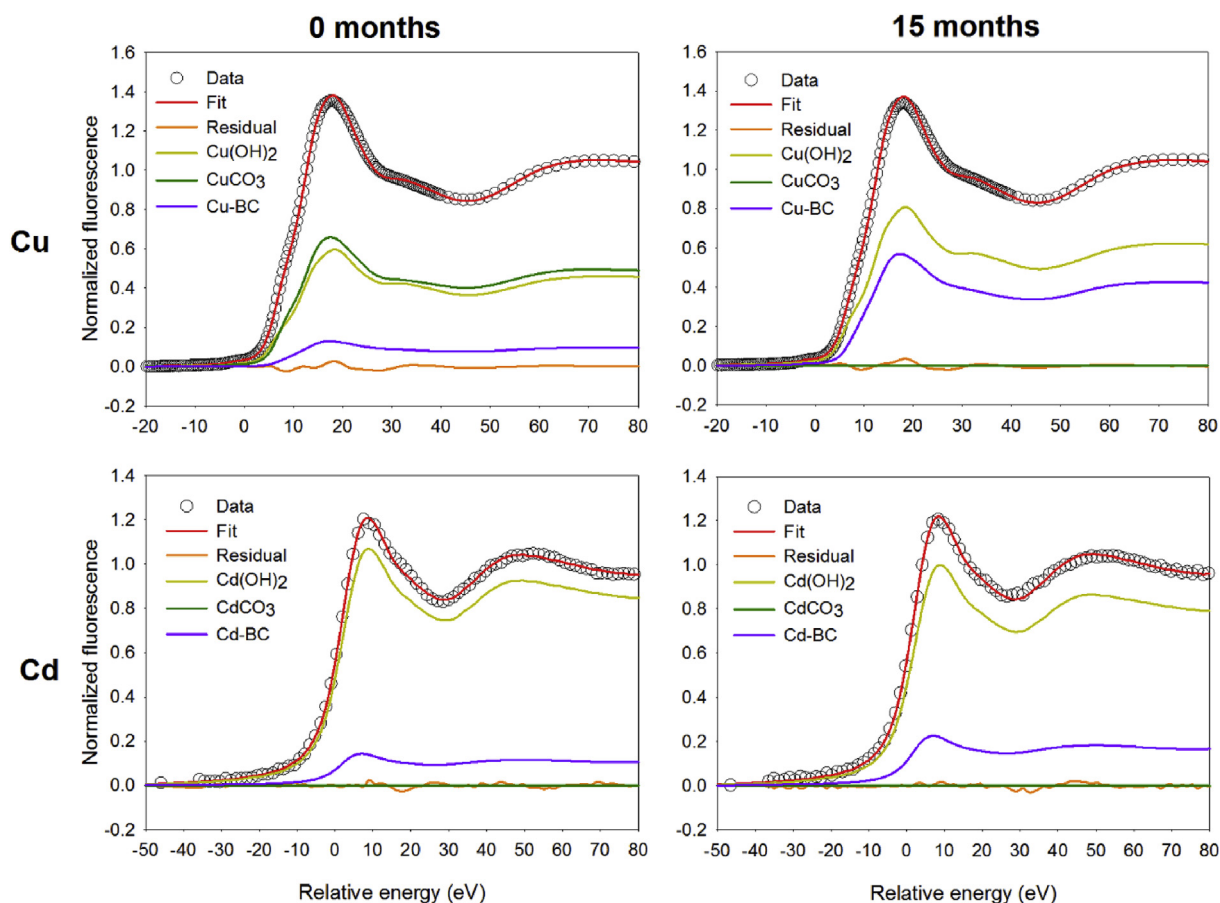


Fig. 6. X-ray absorption near edge structure (XANES) spectra of Cu and Cd bound to fresh (0 months) and aged (15 months) biochars with spectra of respective reference materials.

Table 2

Characterization of wood chip biochar before (0 months) and after aging (15 months) in soil.

	0 months	15 months
Water contact angle [°]	62.4 ± 4.8	4.2 ± 1.5
SSA [m ² g ⁻¹]	88.6 ± 2.5	108.1 ± 2.9
Power law exponent n ^a	3.80 ± 0.02	3.78 ± 0.03
Radius of Gyration ^a [nm]	2.4 ± 0.1	3.1 ± 0.2

^a Obtained by small angle X-ray scattering; SSA = specific surface area (estimated from H₂O adsorption at $p/p_0 = 0.19$).

Table 3

Linear combination fitting (LCF) results for X-ray absorption near edge structure (XANES) spectra of Cu and Cd bound to fresh (0 months) and aged (15 months) biochars. Values given as proportion of reference standards in the samples (%).

BC + Cu	Cu(OH) ₂	CuCO ₃	Cu-BC ^a	EP (×10 ⁻³)
0 months	43.7	47.1	9.2	3.63
15 months	59.3	0	40.7	5.19
BC + Cd	Cd(OH) ₂	CdCO ₃	Cd-BC ^a	EP (×10 ⁻³)
0 months	0	89.0	11.0	3.95
15 months	0	82.7	17.3	4.91

EP = error parameter = $\sum(\text{data-fit})^2/(\text{data})^2$.

^a Biochar standard.

3.3. Cu and Cd sorption mechanisms

MIR spectroscopy was carried out for fresh and aged BCs equilibrated with Cu and Cd solutions at pH 4 and pH 6.3,

respectively. HM sorption led to a shift of the BCs' MIR bands (Fig. S1). Fresh BC equilibrated with Cd at pH 6.3 showed a shift of the peak at 1429 cm⁻¹ (control) to 1433 cm⁻¹ for samples treated with 15 mg L⁻¹ Cd and to 1439 cm⁻¹ for samples treated with 300 mg L⁻¹ Cd, respectively. These shifts could indicate surface-exchange reactions of Cd²⁺ with Ca²⁺ ions at CaCO₃ sites. Similar, but less pronounced shifts were found for aged BC samples (Fig. S1). Furthermore, the bands at 1429–1439 cm⁻¹ and 875 cm⁻¹ were generally more pronounced after metal sorption. This may be attributed to the formation of Cu and Cd complexes with C=O containing functional groups or carbonate (co-)precipitation. After metal sorption at pH 4, a new peak formed at 1384 cm⁻¹, previously attributed to HM adsorption to carboxyl groups on a BC derived from wheat residues (Wang et al., 2011). This peak was more pronounced for aged BCs. Additionally, a shift of the band around 1575 cm⁻¹ (attributed to C=O stretching vibration) towards higher wavenumbers was observed, which indicates complexation of Cu(II) with organic functional groups (Anoop Krishnan et al., 2011; Tong et al., 2011).

In summary, the results of MIR spectroscopy of HM-spiked BC samples revealed that carbonates formed in the BCs may be important HM sorbents even after 15 months of aging in an acidic soil. This observation is congruent with the still elevated pH levels found in the proximity of aged BC particles (Fig. 2). Our results also indicate that BC organic functional groups become more important for HM sorption upon aging, thus supporting our hypothesis 2.

The speciation of sorbed Cu(II) and Cd(II) on fresh and aged BCs was further investigated by means of XAS. XANES spectra of fresh and aged BCs spiked with Cu and Cd, respectively, were collected

and compared to selected reference compounds via LCF (Table 3, Fig. 6). In addition to hydroxide and carbonate, Cu–BC and Cd–BC references (s. supporting information) were used to account for metal complexation to organic functional groups on fused aromatic ring structures in . Our BC standard had been treated with HF–HCl to eliminate silica and oxides (Hsu et al., 2009), and metal sorption was conducted at pH 4, which is below the first hydrolysis constants of the metal ions, in order to avoid precipitation.

LCF suggested that Cu precipitated as $\text{Cu}(\text{OH})_2$ on fresh as well as aged BCs, whereas CuCO_3 was only found for fresh BCs. Aged BCs showed strongly increased Cu(II) complexation to organic functional groups (from 9.2% to 46.7%) as indicated by the Cu–BC standard (see supporting information). This is likely the result of increased functionality due to oxidation processes as well as better accessibility of BC pores and reactive surfaces. As the sorption isotherms had revealed (Fig. 1), Cu sorption was less affected by BC aging processes; this could be because $\text{Cu}(\text{OH})_2$ seems to have readily precipitated already on the fresh alkaline BC surfaces and the surrounding soil. However, the observed shift of Cu binding mechanisms towards the less pH-dependent sorption to BC organic phases is expected to be beneficial for long-term HM immobilization after the BC-induced liming effects have ceased.

In comparison, LCF suggested that the proportion of Cd sorbed to organic sites increased less strongly, from 11% to 17.3%. Carbonate precipitation was suggested by LCF as the major form of Cd immobilization on fresh and aged BCs. CdCO_3 precipitation is not a common process in soils as it requires rather high Cd^{2+} concentrations and alkaline conditions, but was observed on several biochars before (Li et al., 2017). Facilitated by the BC's porous structure that harbors a large portion of its alkalinity, the solution pH in the proximity of BC particles was elevated even after 15 months of soil aging (Fig. 2), which likely facilitated Cu and Cd (co-)precipitation. CaCO_3 is known for its high affinity to adsorb Cu and Cd. Rapid Cd^{2+} adsorption on calcite surfaces is accompanied by a slower, irreversible uptake. The latter was specified as a combination of diffusion of Cd^{2+} into the lattice and growth of otavite (CdCO_3) on calcite by means of a CaCO_3 dissolution - CdCO_3 precipitation reaction (Ahmed et al., 2008; Martin-Garin et al., 2003). CdCO_3 precipitation was found to drastically decrease calcite dissolution rates (formation of a less than $0.01 \mu\text{m}$ thick layer of CdCO_3 decreased calcite dissolution by two orders of magnitude) and hence slowing this process down (Cubillas et al., 2005). Bailey et al. (2005) found ongoing Cd diffusion into calcite even after 9 months reaction time. Our XANES results show that the strongly enhanced sorption of Cd after aging of soil-BC mixtures (cf. Fig. 1) cannot be explained by major shifts in Cd sorption mechanisms. For Cd sorption, the better accessibility of BC pores with therein-precipitated CaCO_3 seems to be the dominant factor that dominated over the overall lower carbonate content and lower pH of the aged BCs.

4. Conclusions

Our study suggests that beside the liming effect that BC amendments usually bring about, the accessibility to the BCs' pore network and reactive surfaces is a decisive factor for effective HM immobilization in contaminated soils and wastewaters. As long as the BC pore network is not fully accessible for aqueous solutions due to hydrophobic surfaces, the BCs cannot develop their full potential for HM immobilization. Once the hydrophobicity of fresh BC has waned, CaCO_3 -containing BC proved very effective for immobilizing Cd in our study. Another recent study investigating a contaminated soil under acid rain conditions also showed that the application of BCs was more effective than liming for the immobilization of Cd (Lu et al., 2015). Our findings suggest that HMs are initially "trapped" by formation of hydroxide and carbonate

precipitates within BC particles and that in the longer term, sorption to organic functional groups takes over and sustains HM immobilization after the initial liming effect has ceased.

MIR spectra of biochars equilibrated with Cu and Cd solutions (Fig. S1), detailed information about EXAFS measurement of the Cu-BC and Cd-BC standards (S1, Fig. S2, Table S1).

Author contributions

The manuscript was written through contributions from all co-authors. All co-authors have given approval to the final version of the manuscript.

Acknowledgements

The authors are grateful to Jyh-Fu Lee, Ting-Shan Chan, Jeng-Lung Chen, Jannis Bückler, Bernhard Wimmer and Christoph Höfer for their help in sample procurement and measurements. This research was carried out in part at the National Synchrotron Radiation Research Center, Hsinchu, Taiwan.

Appendix A. Supplementary data

Supplementary data to this article can be found online at <https://doi.org/10.1016/j.chemosphere.2018.10.094>.

References

- Ahmed, I.A.M., Crout, N.M.J., Young, S.D., 2008. Kinetics of Cd sorption, desorption and fixation by calcite: a long-term radiotracer study. *Geochim. Cosmochim. Acta* 72, 1498–1512. <https://doi.org/10.1016/j.gca.2008.01.014>.
- Ali, H., Khan, E., Sajad, M.A., 2013. Phytoremediation of heavy metals—concepts and applications. *Chemosphere* 91, 869–881. <https://doi.org/10.1016/j.chemosphere.2013.01.075>.
- Alva, A.K., Univ of, F., Sumner, M.E., Miller, W.P., 1991. Relationship between ionic strength and electrical conductivity for soil solutions. *Soil Sci. USA*.
- Álvarez, R., Ordóñez, A., Pérez, A., De Miguel, E., Charlesworth, S., 2018. Mineralogical and environmental features of the Asturian copper mining district (Spain): a review. *Eng. Geol.* 243, 206–217. <https://doi.org/10.1016/j.enggeo.2018.07.007>.
- Anoop Krishnan, K., Sreejalekshmi, K.G., Baiju, R.S., 2011. Nickel(II) adsorption onto biomass based activated carbon obtained from sugarcane bagasse pith. *Bioresour. Technol.* 102, 10239–10247. <https://doi.org/10.1016/j.biortech.2011.08.069>.
- Bailey, E.H., Mosselmans, J.F.W., Young, S.D., 2005. Time-dependent surface reactivity of Cd sorbed on calcite, hydroxylapatite and humic acid. *Mineral. Mag.* 69, 563–575. <https://doi.org/10.1180/0026461056950271>.
- Barros, N., Salgado, J., Feijóo, S., 2007. Calorimetry and Soil. *Thermochim. Acta*, XIVth ISBC Proceedings Special Issue, vol. 458, pp. 11–17. <https://doi.org/10.1016/j.tca.2007.01.010>.
- Beesley, L., Marmiroli, M., 2011. The immobilisation and retention of soluble arsenic, cadmium and zinc by biochar. *Environ. Pollut.* 159, 474–480. <https://doi.org/10.1016/j.envpol.2010.10.016>.
- Beesley, L., Moreno-Jiménez, E., Gomez-Eyles, J.L., 2010. Effects of biochar and greenwaste compost amendments on mobility, bioavailability and toxicity of inorganic and organic contaminants in a multi-element polluted soil. *Environ. Pollut.* 158, 2282–2287. <https://doi.org/10.1016/j.envpol.2010.02.003>.
- Blackwell, P., Riethmuller, G., Collins, M., 2009. Biochar application to soil. In: Lehmann, J., Joseph, S. (Eds.), *Biochar for Environmental Management: Science and Technology*. Earthscan, London, pp. 183–206.
- Brun, L., Maillet, J., Hinsinger, P., Pépin, M., 2001. Evaluation of copper availability to plants in copper-contaminated vineyard soils. *Environ. Pollut.* 111, 293–302. [https://doi.org/10.1016/S0269-7491\(00\)00667-1](https://doi.org/10.1016/S0269-7491(00)00667-1).
- Cheng, C.-H., Lehmann, J., Engelhard, M.H., 2008. Natural oxidation of black carbon in soils: changes in molecular form and surface charge along a climosequence. *Geochim. Cosmochim. Acta* 72, 1598–1610. <https://doi.org/10.1016/j.gca.2008.01.010>.
- Cheng, C.-H., Lehmann, J., Thies, J.E., Burton, S.D., Engelhard, M.H., 2006. Oxidation of black carbon by biotic and abiotic processes. *Org. Geochem.* 37, 1477–1488. <https://doi.org/10.1016/j.orggeochem.2006.06.022>.
- Cheraghi, M., Lorestani, B., Merrikhpour, H., 2012. Investigation of the effects of phosphate fertilizer application on the heavy metal content in agricultural soils with different cultivation patterns. *Biol. Trace Elem. Res.* 145, 87–92. <https://doi.org/10.1007/s12011-011-9161-3>.
- Chia, C.H., Gong, B., Joseph, S.D., Marjo, C.E., Munroe, P., Rich, A.M., 2012. Imaging of mineral-enriched biochar by FTIR, Raman and SEM–EDX. *Vib. Spectrosc.* 62,

- 248–257. <https://doi.org/10.1016/j.vibspec.2012.06.006>.
- Conte, P., Nestle, N., 2015. Water dynamics in different biochar fractions. *Magn. Reson. Chem.* 53, 726–734. <https://doi.org/10.1002/mrc.4204>.
- Conte, P., Schmidt, H.-P., 2017. Soil-water interactions unveiled by fast field cycling NMR relaxometry. In: Harris, R.K., Wasylishen, R.L. (Eds.), *EMagRes*. John Wiley & Sons, Ltd, Chichester, UK, pp. 453–464. <https://doi.org/10.1002/9780470034590.emrstm1535>.
- Cubillas, P., Köhler, S., Prieto, M., Causserand, C., Oelkers, E.H., 2005. How do mineral coatings affect dissolution rates? An experimental study of coupled CaCO₃ dissolution—CdCO₃ precipitation. *Geochim. Cosmochim. Acta* 69, 5459–5476. <https://doi.org/10.1016/j.gca.2005.07.016>.
- Das, O., Sarmah, A.K., 2015. The love–hate relationship of pyrolysis biochar and water: a perspective. *Sci. Total Environ.* 512 (513), 682–685. <https://doi.org/10.1016/j.scitotenv.2015.01.061>.
- Fang, L., Borggaard, O.K., Marcussen, H., Holm, P.E., Bruun Hansen, H.C., 2010. The pH-dependent adsorption of tributyltin to charcoals and soot. *Environ. Pollut.* 158, 3642–3649. <https://doi.org/10.1016/j.envpol.2010.08.003>.
- Fang, Q., Chen, B., Lin, Y., Guan, Y., 2014. Aromatic and hydrophobic surfaces of wood-derived biochar enhance perchlorate adsorption via hydrogen bonding to oxygen-containing organic groups. *Environ. Sci. Technol.* 48, 279–288. <https://doi.org/10.1021/es403711y>.
- Gibaud, A., Xue, J.S., Dahn, J.R., 1996. A small angle X-ray scattering study of carbons made from pyrolyzed sugar. *Carbon* 34, 499–503. [https://doi.org/10.1016/0008-6223\(95\)00207-3](https://doi.org/10.1016/0008-6223(95)00207-3).
- Guo, Y., Bustin, R.M., 1998. FTIR spectroscopy and reflectance of modern charcoals and fungal decayed woods: implications for studies of inertinite in coals. *Int. J. Coal Geol.* 37, 29–53. [https://doi.org/10.1016/S0166-5162\(98\)00019-6](https://doi.org/10.1016/S0166-5162(98)00019-6).
- Haberhauer, G., Gerzabek, M.H., 1999. Drift and transmission FT-IR spectroscopy of forest soils: an approach to determine decomposition processes of forest litter. *Vib. Spectrosc.* 19, 413–417. [https://doi.org/10.1016/S0924-2031\(98\)00046-0](https://doi.org/10.1016/S0924-2031(98)00046-0).
- Hagemann, N., Joseph, S., Schmidt, H.-P., Kammann, C.L., Harter, J., Borcher, T., Young, R.B., Varga, K., Taherymoosavi, S., Elliott, K.W., McKenna, A., Albu, M., Mayrhofer, C., Obst, M., Conte, P., Dieguez-Alonso, A., Orsetti, S., Subdiaga, E., Behrens, S., Kappler, A., 2017. Organic coating on biochar explains its nutrient retention and stimulation of soil fertility. *Nat. Commun.* 8, 1089. <https://doi.org/10.1038/s41467-017-01123-0>.
- Hoefler, C., Santner, J., Borisov, S.M., Wenzel, W.W., Puschenreiter, M., 2017. Integrating chemical imaging of cationic trace metal solutes and pH into a single hydrogel layer. *Anal. Chim. Acta* 950, 88–97. <https://doi.org/10.1016/j.aca.2016.11.004>.
- Hsu, N.-H., Wang, S.-L., Lin, Y.-C., Sheng, G.D., Lee, J.-F., 2009. Reduction of Cr(VI) by crop-residue-derived black carbon. *Environ. Sci. Technol.* 43, 8801–8806. <https://doi.org/10.1021/es901872x>.
- Jarup, L., 2003. Hazards of heavy metal contamination. *Br. Med. Bull.* 68, 167–182. <https://doi.org/10.1093/bmb/ldg032>.
- Kaal, J., Martínez Cortizas, A., Reyes, O., Soliño, M., 2012. Molecular characterization of Ulex europaeus biochar obtained from laboratory heat treatment experiments – a pyrolysis–GC/MS study. *J. Anal. Appl. Pyrolysis* 95, 205–212. <https://doi.org/10.1016/j.jaap.2012.02.008>.
- Keiluweit, M., Nico, P.S., Johnson, M.G., Kleber, M., 2010. Dynamic molecular structure of plant biomass-derived black carbon (biochar). *Environ. Sci. Technol.* 44, 1247–1253. <https://doi.org/10.1021/es9031419>.
- Kloss, S., Zehetner, F., Buecker, J., Oburger, E., Wenzel, W.W., Enders, A., Lehmann, J., Soja, G., 2015. Trace element biogeochemistry in the soil-water-plant system of a temperate agricultural soil amended with different biochars. *Environ. Sci. Pollut. Res.* 22, 4513–4526. <https://doi.org/10.1007/s11356-014-3685-y>.
- Kloss, S., Zehetner, F., Dellantonio, A., Hamid, R., Ottner, F., Liedtke, V., Schwanninger, M., Gerzabek, M.H., Soja, G., 2012. Characterization of slow pyrolysis biochars: effects of feedstocks and pyrolysis temperature on biochar properties. *J. Environ. Qual.* 41, 990. <https://doi.org/10.2134/jeq2011.0070>.
- Kloss, S., Zehetner, F., Wimmer, B., Buecker, J., Rempt, F., Soja, G., 2014. Biochar application to temperate soils: effects on soil fertility and crop growth under greenhouse conditions. *J. Plant Nutr. Soil Sci.* 177, 3–15. <https://doi.org/10.1002/jpln.201200282>.
- Koch, A., 1998. A study of carbonaceous char oxidation in air by semi-quantitative FTIR spectroscopy. *Fuel* 77, 563–569. [https://doi.org/10.1016/S0016-2361\(97\)00157-9](https://doi.org/10.1016/S0016-2361(97)00157-9).
- Komárek, M., Čadková, E., Chrástný, V., Bordas, F., Bollinger, J.-C., 2010. Contamination of vineyard soils with fungicides: a review of environmental and toxicological aspects. *Environ. Int.* 36, 138–151. <https://doi.org/10.1016/j.envint.2009.10.005>.
- Lamichhane, J.R., Osdaghi, E., Behlau, F., Köhl, J., Jones, J.B., Aubertot, J.-N., 2018. Thirteen decades of antimicrobial copper compounds applied in agriculture. A review. *Agron. Sustain. Dev.* 38, 28. <https://doi.org/10.1007/s13593-018-0503-9>.
- Li, H., Dong, X., da Silva, E.B., de Oliveira, L.M., Chen, Y., Ma, L.Q., 2017. Mechanisms of metal sorption by biochars: biochar characteristics and modifications. *Chemosphere* 178, 466–478. <https://doi.org/10.1016/j.chemosphere.2017.03.072>.
- Li, H., Ye, X., Geng, Z., Zhou, H., Guo, X., Zhang, Y., Zhao, H., Wang, G., 2016. The influence of biochar type on long-term stabilization for Cd and Cu in contaminated paddy soils. *J. Hazard Mater.* 304, 40–48. <https://doi.org/10.1016/j.jhazmat.2015.10.048>.
- Lu, H., Li, Z., Fu, S., Méndez, A., Gascó, G., Paz-Ferreiro, J., 2015. Effect of biochar in cadmium availability and soil biological activity in an anthrosol following acid rain deposition and aging. *Water Air Soil Pollut.* 226, 164. <https://doi.org/10.1007/s11270-015-2401-y>.
- Martin-Garin, A., Van Cappellen, P., Charlet, L., 2003. Aqueous cadmium uptake by calcite: a stirred flow-through reactor study. *Geochim. Cosmochim. Acta* 67, 2763–2774. [https://doi.org/10.1016/S0016-7037\(03\)00091-7](https://doi.org/10.1016/S0016-7037(03)00091-7).
- Nagodavithane, C.L., Singh, B., Fang, Y., 2014. Effect of ageing on surface charge characteristics and adsorption behaviour of cadmium and arsenate in two contrasting soils amended with biochar. *Soil Res.* 52, 155. <https://doi.org/10.1071/SR13187>.
- Pfeifer, P., Ehrburger-Dolle, F., Rieker, T.P., González, M.T., Hoffman, W.P., Molina-Sabio, M., Rodríguez-Reinoso, F., Schmidt, P.W., Voss, D.J., 2002. Nearly space-filling fractal networks of carbon nanopores. *Phys. Rev. Lett.* 88. <https://doi.org/10.1103/PhysRevLett.88.115502>.
- Quirk, J.P., 1955. Significance of surface areas calculated from water vapor sorption isotherms by use of the B.E.T. equation. *Soil Sci.* 80, 423.
- Quirk, J.P., Murray, R.S., 1999. Appraisal of the ethylene glycol monoethyl ether method for measuring hydratable surface area of clays and soils. *Soil Sci. Soc. Am. J.* 63, 839–849. <https://doi.org/10.2136/sssaj1999.634839x>.
- Ravel, B., Newville, M., 2005. ATHENA, ARTEMIS, HEPHAESTUS: data analysis for X-ray absorption spectroscopy using IFEFFIT. *J. Synchrotron Radiat.* 12, 537–541. <https://doi.org/10.1107/S0909049505012719>.
- Rechberger, M.V., Kloss, S., Rennhofer, H., Tintner, J., Watzinger, A., Soja, G., Lichtenegger, H., Zehetner, F., 2017. Changes in biochar physical and chemical properties: accelerated biochar aging in an acidic soil. *Carbon* 115, 209–219. <https://doi.org/10.1016/j.carbon.2016.12.096>.
- Rizwan, M., Ali, S., Zia ur Rehman, M., Rinklebe, J., Tsang, D.C.W., Bashir, A., Maqbool, A., Tack, F.M.G., Ok, Y.S., 2018. Cadmium phytoremediation potential of Brassica crop species: a review. *Sci. Total Environ.* 631–632, 1175–1191. <https://doi.org/10.1016/j.scitotenv.2018.03.104>.
- Rumpel, C., Janik, L.J., Skjemstad, J.O., Kögel-Knabner, I., 2001. Quantification of carbon derived from lignite in soils using mid-infrared spectroscopy and partial least squares. *Org. Geochem.* 32, 831–839. [https://doi.org/10.1016/S0146-6380\(01\)00029-8](https://doi.org/10.1016/S0146-6380(01)00029-8).
- Sahouli, B., Blacher, S., Brouers, F., Sobry, R., Van den Bossche, G., Diez, D., Darmstadt, H., Roy, C., Kaliaguine, S., 1996. Surface morphology of commercial carbon blacks and carbon blacks from pyrolysis of used tyres by small-angle X-ray scattering. *Carbon* 34, 633–637. [https://doi.org/10.1016/0008-6223\(96\)00017-6](https://doi.org/10.1016/0008-6223(96)00017-6).
- Sauvé, S., Hendershot, W., Allen, H.E., 2000. Solid-solution partitioning of metals in contaminated soils: dependence on pH, total metal burden, and organic matter. *Environ. Sci. Technol.* 34, 1125–1131. <https://doi.org/10.1021/es9907764>.
- Smith, N.J., 1980. Anthrosols and human carrying capacity in amazonia. *Ann. Assoc. Am. Geogr.* 70, 553–566. <https://doi.org/10.1111/j.1467-8306.1980.tb01332.x>.
- Socrates, G., 2001. *Infrared and Raman Characteristic Group Frequencies: Tables and Charts*. John Wiley & Sons.
- Stevenson, F.J., 1994. *Humus Chemistry: Genesis, Composition, Reactions*, second ed. John Wiley & Sons.
- Tatzber, M., Stemmer, M., Spiegel, H., Katzlberger, C., Haberhauer, G., Mentler, A., Gerzabek, M.H., 2007. FTIR-spectroscopic characterization of humic acids and humin fractions obtained by advanced NaOH, Na₄P₂O₇, and Na₂CO₃ extraction procedures. *J. Plant Nutr. Soil Sci.* 170, 522–529. <https://doi.org/10.1002/jpln.200622082>.
- Toles, C.A., Marshall, W.E., Johns, M.M., 1999. Surface functional groups on acid-activated nutshell carbons. *Carbon* 37, 1207–1214. [https://doi.org/10.1016/S0008-6223\(98\)00315-7](https://doi.org/10.1016/S0008-6223(98)00315-7).
- Tong, X., Li, J., Yuan, J., Xu, R., 2011. Adsorption of Cu(II) by biochars generated from three crop straws. *Chem. Eng. J.* 172, 828–834. <https://doi.org/10.1016/j.cej.2011.06.069>.
- Uchimiya, M., Bannon, D.I., Wartelle, L.H., 2012. Retention of heavy metals by carboxyl functional groups of biochars in small arms range soil. *J. Agric. Food Chem.* 60, 1798–1809. <https://doi.org/10.1021/jf2047898>.
- Uchimiya, M., Lima, I.M., Thomas Klasson, K., Chang, S., Wartelle, L.H., Rodgers, J.E., 2010. Immobilization of heavy metal ions (Cu^{II}, Cd^{II}, Ni^{II}, and Pb^{II}) by broiler litter-derived biochars in water and soil. *J. Agric. Food Chem.* 58, 5538–5544. <https://doi.org/10.1021/jf9044217>.
- Wacha, A., Varga, Z., Vainio, U., Hoell, A., Bóta, A., 2011. Small-angle X-ray scattering experiments and computer simulations to characterise anisotropy of activated carbons prepared from wood. *Carbon* 49, 3958–3971. <https://doi.org/10.1016/j.carbon.2011.05.035>.
- Wang, X.S., Miao, H.H., He, W., Shen, H.L., 2011. Competitive adsorption of Pb(II), Cu(II), and Cd(II) ions on wheat-residue derived black carbon. *J. Chem. Eng. Data* 56, 444–449. <https://doi.org/10.1021/je101079w>.
- Watzinger, A., Feichtmair, S., Kitzler, B., Zehetner, F., Kloss, S., Wimmer, B., Zechmeister-Boltenstern, S., Soja, G., 2014. Soil microbial communities responded to biochar application in temperate soils and slowly metabolized ¹³C-labelled biochar as revealed by ¹³C PLFA analyses: results from a short-term incubation and pot experiment. *Eur. J. Soil Sci.* 65, 40–51. <https://doi.org/10.1111/ejss.12100>.
- Woolf, D., Amonette, J.E., Street-Perrott, F.A., Lehmann, J., Joseph, S., 2010. Sustainable biochar to mitigate global climate change. *Nat. Commun.* 1, 56. <https://doi.org/10.1038/ncomms1053>.
- Yi, S., Witt, B., Chiu, P., Guo, M., Imhoff, P., 2015. The origin and reversible nature of poultry litter biochar hydrophobicity. *J. Environ. Qual.* 44, 963–971. <https://doi.org/10.2134/jeq2014.09.0385>.